Low-lying excitations of vortex lattices in condensates with anisotropic dipole-dipole interaction

Lijuan Jia,[1,2] An-Bang Wang,[1,2] and Su Yi[1,2,3]

[1]*CAS Key Laboratory of Theoretical Physics, Institute of Theoretical Physics, Chinese Academy of Sciences, Beijing 100190, China*

[2]*School of Physical Sciences, University of Chinese Academy of Sciences, Beijing 100049, China*

[3]*CAS Center for Excellence in Topological Quantum Computation, University of Chinese Academy of Sciences, Beijing 100190, China*

(Received 4 January 2018; published 16 April 2018)

We investigated the low-lying collective excitations of quasi-two-dimensional dipolar Bose-Einstein condensates confined in a rotating harmonic potential using the Bogoliubov–de Gennes equation. By varying the trap rotation frequency and dipolar interaction strength, we show how the anisotropic dipole-dipole interaction modifies the collective excitations of the condensates. In particular, under strong dipolar interaction, the vortex-displacement excitations differ significantly from the nondipolar case.

DOI: 10.1103/PhysRevA.97.043614

I. INTRODUCTION

Owing to the fundamental importance of topological excitations, the dynamics of quantized vortices has been of interest in a wide variety of physical systems [1,2], ranging from superfluid ^{4}He and ^{3}He to superconductors, quantum magnets, liquid crystals, nuclear matter, and nonlinear optical systems [3]. The realizations of quantized vortices and vortex lattices in Bose-Einstein condensates (BECs) of neutral atoms [4–8] stimulated extensive studies on the properties of the vortex states [9]. More importantly, the unprecedented tunability of atomic gases allows a detailed study on the collective excitations of the vortex states. Of particular interest, a vortex lattice supports the so-called Tkachenko waves, namely, the vortex displacement waves in the vortex array propagating in a direction transverse to the vortex lines [10]. Tkachenko waves were observed in superfluid helium [11] and in the BEC of Rb atoms [12].

In the context of atomic BECs, Tkachenko excitations were further investigated theoretically [13–18]. However, the studies of the collective excitations of many-vortex states in atomic BECs have been mainly focused on systems with short-range interactions. Since the experimental realizations of BECs of atoms with large magnetic dipole moments [19–22], there have been considerable theoretical investigations on the vortex states in rotating dipolar condensates [23–35]. In the presence of the dipole-dipole interaction (DDI), it was found that the vortex lattices may significantly deviate from the normal triangular lattice in nondipolar condensates [23,24]. In particular, Yi and Pu showed that the vortex cores become anisotropic if the DDI is anisotropic on the plane perpendicular to the rotation axis [25]. Moreover, Mulkerin *et al.* calculated that the effective vortex-vortex interaction also becomes anisotropic [26]. Interestingly, Wilson *et al.* studied the stability and excitations of single-vortex states in dipolar condensates by numerically solving the Bogoliubov–de Gennes (BdG) equations [27], which is highly nontrivial in the presence of the long-range interaction. Such equations were first solved numerically by Ronen *et al.* in order to study the Bogoliubov modes of a trapped BEC [36] and also by Martin and Blakie with a modified numerical procedure [37]. However, to our knowledge, we are not aware of any studies on the Tkachenko excitations in rotating dipolar BECs. This naturally leads to the question of how the anisotropic DDI modifies the collective excitations of the vortex lattices.

In this work, we investigate the low-lying collective excitations of vortex arrays in dipolar condensates rotating around the z axis. We shall focus on the quasi-two-dimensional (quasi-2D) geometry by assuming a highly oblate trapping potential. As a result, the Kelvin excitations are not covered here. We further assume that the dipole moments of the atoms are polarized along the x axis such that the DDI in the xy plane is anisotropic. For vortex configurations under different rotation frequencies, we show how the DDI modifies the collective excitations of the condensates.

Of particular interest, in the strong DDI limit and under sufficiently large rotation frequencies, vortices in the condensate form stripe lattices such that the intervortex spacing along the x axis is smaller than that along the y axis. For the lowest few excitations, each row of vortices behaves as a rigid body which only executes horizontal oscillation. As a result, these excitations represent the shearing motions between neighboring rows. Moreover, for excitations with higher energy, vortex-displacement modes (VDMs) can couple to surface modes due to the anisotropic DDI.

This paper is organized as follows. In Sec. II, we introduce our model and outline the BdG theory for dipolar condensates. In Sec. III, we study the DDI strengh dependence of the excitation spectra under various rotation frequencies. Finally, we conclude in Sec. IV.

II. FORMULATION

We consider a BEC of N polarized dipoles trapped in an axially symmetric potential

$$V_{\rm ho}(\mathbf{r}) = \tfrac{1}{2}m\left(\omega_\perp^2 x^2 + \omega_\perp^2 y^2 + \omega_z^2 z^2\right), \tag{1}$$

where $\omega_\perp$ and ω_z are the radial and axial trap frequencies, respectively. To generate vortices, the trapping potential rotates around the z axis with rotation frequency Ω. The

particle-particle interaction potential includes the s-wave collision and the dipole-dipole interaction:

$$V_{\rm int}(\mathbf{r}-\mathbf{r}') = \frac{4\pi\hbar^2 a_s}{m}\delta(\mathbf{r}-\mathbf{r}') + f\frac{\mu_0\mu^2}{4\pi}\frac{1-3(\hat{\mathbf{d}}\cdot\hat{\mathbf{e}})^2}{|\mathbf{r}-\mathbf{r}'|^3}, \tag{2}$$

where m is the mass of the particle, a_s is the s-wave scattering length, μ_0 is the vacuum permeability, μ is the magnetic dipole moment, $\hat{\mathbf{d}}$ is a unit vector along the direction of the polarized dipole moments, and $\hat{\mathbf{e}} = (\mathbf{r}-\mathbf{r}')/|\mathbf{r}-\mathbf{r}'|$. Finally, f is a factor continuously tunable between $-1/2$ and 1 through a fast rotating orienting field [38]. In this work, we shall only cover the $f \geqslant 0$ region.

Within the mean-field treatment, the condensate wave function Ψ satisfies the Gross-Pitaevskii equation (GPE) which, in the frame corotating with the trapping potential, reads

$$i\frac{\partial\Psi}{\partial t} = \Bigg[-\frac{1}{2}\nabla^2 + \frac{1}{2}(x^2+y^2+\lambda^2 z^2) + \frac{4\pi N a_s}{a_\perp}|\Psi(\mathbf{r})|^2 + g_d\int d\mathbf{r}'\frac{1-3(\hat{\mathbf{d}}\cdot\hat{\mathbf{e}})^2}{|\mathbf{r}-\mathbf{r}'|^3}|\Psi(\mathbf{r}')|^2 - \Omega L_z\Bigg]\Psi, \tag{3}$$

where $\lambda = \omega_z/\omega_\perp$ is the trap aspect ratio, $g_d = fN\mu_0\mu^2/(4\pi\hbar\omega_\perp a_\perp^3)$, Ω (<1) is the rotation frequency of the trapping potential, L_z is the z component of the orbital angular momentum operator, and the wave function Ψ is normalized to unit. Here we have expressed Eq. (3) in the dimensionless form by adopting the following dimensionless units: $a_\perp = \sqrt{\hbar/(m\omega_\perp)}$ for length, $\hbar\omega_\perp$ for energy, $\omega_\perp^{-1}$ for time, $\sqrt{N/a_\perp^3}$ for wave function, and $\omega_\perp$ for frequency.

As we are mainly interested in the Tkachenko modes in this work, it is convenient to focus on the highly oblate traps with $\lambda \gg 1$. The condensate can then be treated as a quasi-2D one, for which the motion along the z axis is frozen to the ground state of the axial harmonic oscillator. As a result, we decompose the condensate wave function into $\Psi(\mathbf{r},t) = \psi(\boldsymbol{\rho},t)\phi(z)$, where $\boldsymbol{\rho} = (x,y)$ and $\phi(z) = (\lambda/\pi)^{1/4}e^{-\lambda z^2/2}$. Multiplying both sides of Eq. (3) from the left by $\phi^*(z)$ and integrating out the z variable, we obtain the 2D GPE

$$i\frac{\partial\psi(\boldsymbol{\rho})}{\partial t} = [H_0 + g_0|\psi(\boldsymbol{\rho})|^2 + g_d\mathcal{D}(\boldsymbol{\rho})]\psi(\boldsymbol{\rho}), \tag{4}$$

where we have defined the 2D single-particle Hamiltonian

$$H_0 = -\tfrac{1}{2}\nabla_\perp^2 + \tfrac{1}{2}\boldsymbol{\rho}^2 - \Omega L_z, \tag{5}$$

$g_0 = 2(2\pi\lambda)^{1/2}Na_s/a_\perp$, and

$$\mathcal{D}(\boldsymbol{\rho}) = \int d\boldsymbol{\rho}' U(\boldsymbol{\rho}-\boldsymbol{\rho}')|\psi(\boldsymbol{\rho}')|^2 \tag{6}$$

is the mean field induced by the DDI, with

$$U(\boldsymbol{\rho}-\boldsymbol{\rho}') = \int dz|\phi(z)|^2\int dz'\frac{1-3(\hat{\mathbf{d}}\cdot\hat{\mathbf{e}})^2}{|\mathbf{r}-\mathbf{r}'|^3}|\phi(z')|^2$$

being the effective 2D dipolar interaction.

In general, the ground-state wave function $\psi_0(\boldsymbol{\rho})$ can be obtained by numerically evolving Eq. (4) in imaginary time. It is worthwhile to point out that $\mathcal{D}(\boldsymbol{\rho})$ can be efficiently evaluated in the momentum space by using the fast Fourier transform. To see this, we make use of the convolution theorem to Eq. (6), which leads to

$$\mathcal{D}(\boldsymbol{\rho}) = \frac{4\pi}{3}\int dz|\phi(z)|^2\mathcal{F}^{-1}[(3(\hat{\mathbf{d}}\cdot\hat{\mathbf{k}})^2-1)\mathcal{F}[|\Psi(\mathbf{r})|^2]],$$

where $\mathcal{F}[\cdot]$ and $\mathcal{F}^{-1}[\cdot]$ denote the Fourier and inverse Fourier transforms, respectively, and we have used the fact that

$$\mathcal{F}\left[\frac{1-3(\hat{\mathbf{d}}\cdot\hat{\mathbf{r}})^2}{|\mathbf{r}|^3}\right] = \frac{4\pi}{3}[3(\hat{\mathbf{d}}\cdot\hat{\mathbf{k}})^2-1]. \tag{7}$$

Straightforward calculation then gives rise to

$$\mathcal{D}(\boldsymbol{\rho}) = \mathcal{F}_\perp^{-1}[\widetilde{U}(\mathbf{k}_\rho)\mathcal{F}_\perp[|\psi(\boldsymbol{\rho})|^2]], \tag{8}$$

where $\mathcal{F}_\perp[\cdot]$ and $\mathcal{F}_\perp^{-1}[\cdot]$ represent the Fourier and inverse Fourier transforms in the xy plane, respectively, and

$$\widetilde{U}(\mathbf{k}_\rho) = -\frac{2}{3}\int dk_z e^{-k_z^2/(2\lambda)}[1-3(\hat{\mathbf{d}}\cdot\hat{\mathbf{k}})^2], \tag{9}$$

where $\mathbf{k}_\rho = (k_x,k_y)$. In particular, for $\hat{\mathbf{d}} = \hat{\mathbf{x}}$, we have

$$\widetilde{U}(\mathbf{k}_\rho) = \frac{4\pi}{3}\sqrt{\frac{\lambda}{2}}\left[\frac{-1}{\sqrt{\pi}} + 3\frac{\bar{k}_x^2}{\bar{k}_\rho}e^{\bar{k}_\rho^2}\mathrm{erfc}(\bar{k}_\rho)\right],$$

where $\bar{k}_x = k_x/\sqrt{2\lambda}$, $\bar{k}_\rho = \sqrt{(k_x^2+k_y^2)/(2\lambda)}$, and $\mathrm{erfc}(\cdot)$ is the complementary error function. For simplicity, we further assume that all dipole moments are polarized along the x axis such that the dipolar interaction in the quasi-2D system is anisotropic, i.e., attractive (repulsive) along the x (y) direction. However, it should be noted that overall dipolar interaction for the quasi-2D condensate is always attractive.

Once the ground-state wave function $\psi_0(\boldsymbol{\rho})$ is found, we may study the collective excitations of the condensate by employing the Bogoliubov–de Gennes theory. Specifically, we expand the wave function into

$$\psi(\boldsymbol{\rho},t) = [\psi_0(\boldsymbol{\rho}) + p\vartheta(\boldsymbol{\rho},t)]e^{-i\mu t}, \tag{10}$$

where μ is the chemical potential of the ground state, $p \ll 1$ is a small quantity used to control the population of quasiparticle excitation, and $\vartheta(\boldsymbol{\rho},t)$ is expanded as

$$\vartheta(\boldsymbol{\rho},t) = \sum_j[u_j(\boldsymbol{\rho})e^{-i\omega_j t} + v_j^*(\boldsymbol{\rho})e^{i\omega_j t}], \tag{11}$$

with (u_j,v_j^*) being the modes of the excitations and ω_j the corresponding frequencies. Here mode functions are normalized as

$$\int d\boldsymbol{\rho}[|u_j(\boldsymbol{\rho})|^2 - |v_j(\boldsymbol{\rho})|^2] = 1. \tag{12}$$

After inserting Eqs. (10) and (11) into Eq. (4), we equate terms evolving in time according to $e^{-i\omega_j t}$ and $e^{i\omega_j t}$, respectively, which leads to the coupled BdG equations

$$\begin{pmatrix}\mathcal{L}_{11} & \mathcal{L}_{12}\\ \mathcal{L}_{21} & \mathcal{L}_{22}\end{pmatrix}\begin{pmatrix}u_j\\ v_j\end{pmatrix} = \omega_j\begin{pmatrix}u_j\\ v_j\end{pmatrix}, \tag{13}$$

where

$$\mathcal{L}_{11} = \mathcal{L}_{\rm GP} - \mu + g_0|\psi_0|^2 + g_d\hat{\chi}_1 = -\mathcal{L}_{22}^*,$$
$$\mathcal{L}_{12} = g_0\psi_0^2 + g_d\hat{\chi}_2 = -\mathcal{L}_{21}^*,$$

with $\mathcal{L}_{\rm GP} = -\frac{1}{2}\nabla_\perp^2 + \frac{1}{2}\boldsymbol{\rho}^2 + g_0|\psi_0(\boldsymbol{\rho})|^2 + g_d U_{\mathbf{d}}(\boldsymbol{\rho}) - \Omega L_z$. Furthermore, the actions of the operators $\hat{\chi}_1$ and $\hat{\chi}_2$ on a function f are defined, respectively, as

$$(\hat{\chi}_1 f)(\boldsymbol{\rho}) = \psi_0(\boldsymbol{\rho}) \int d\boldsymbol{\rho}' U_{\mathbf{d}}(\boldsymbol{\rho} - \boldsymbol{\rho}')\psi_0^*(\boldsymbol{\rho}')f(\boldsymbol{\rho}')$$

and

$$(\hat{\chi}_2 f)(\boldsymbol{\rho}) = \psi_0(\boldsymbol{\rho}) \int d\boldsymbol{\rho}' U_{\mathbf{d}}(\boldsymbol{\rho} - \boldsymbol{\rho}')\psi_0(\boldsymbol{\rho}')f(\boldsymbol{\rho}').$$

Following Ref. [36], we solve the BdG equations (13) with the Arnoldi method by employing ARPACK [39], which gives rise to the eigenfrequencies ω_j and eigenmodes (u_j, v_j). To visualize a normal mode, we analyze the evolution of the perturbed density profile

$$n_p(\boldsymbol{\rho},t) = |\psi_0(\boldsymbol{\rho}) + p[u_j(\boldsymbol{\rho})e^{-i\omega_j t} + v_j^*(\boldsymbol{\rho})e^{i\omega_j t}]|^2, \quad (14)$$

which reveals the nature of the excitations.

For the numerical results presented below, we consider a condensate of $N = 3 \times 10^4$ Cr atoms [19]. We assume that the s-wave scattering length of the Cr atom is tuned to $a_s = 2.83$ nm via Feshbach. The radial trap frequency is taken to be $\omega_\perp = (2\pi)100$ Hz and the trap aspect ratio is $\lambda = 10$. With these specifications, the dimensionless contact interaction strength becomes $g_0 \simeq 966$ which, for simplicity, is fixed in all numerical calculations. Consequently, the free parameters of the system reduce to the dimensionless the interaction strength g_d and the rotation frequency Ω. By noting that the magnetic dipole moment of the Cr atom is 6 Bohr magneton, it can be easily shown that the interaction ratio g_d/g_0 may range from 0 to 0.2, a region that shall be covered by the numerical computations. In fact, with the help of Feshbach resonance, this parameter regime is also experimentally accessible in both Dy and Er condensates [21,22].

III. RESULTS

A. General structures of the excitation spectra

To explore the structure of the excitation spectrum, we first consider a simpler case corresponding to a rather small rotation frequency $\Omega = 0.3$. Figure 1 plots the frequencies of the low-lying excitations as a function of the dipolar interaction

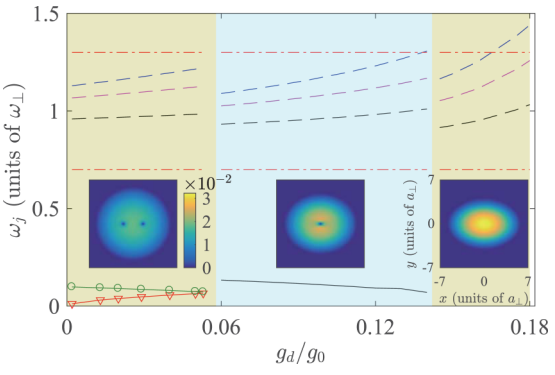

FIG. 1. Frequencies of the low-lying excitations versus the dipolar interaction strength for rotation frequency $\Omega = 0.3$. From left to right, the insets show the density profiles of the ground states corresponding to $g_d/g_0 = 0.02$, 0.12, and 0.16, respectively.

strength. Clearly, according to the behavior of the excitation spectra, the g_d axis is divided into three regions which, as shown in the insets, correspond to three different types of ground states. In the weak DDI region, the condensate contains $N_v = 2$ vortices. As one increases g_d, these two vortices move away from each other and for sufficiently large g_d the vortex number reduces to 1. Eventually, the condensate becomes free of vortex for sufficiently large g_d. In addition, the condensate collapses when $g_d > 0.18g_0$. The underlying reason for the decrease of N_v with growing g_d is because the overall DDI in the quasi-2D condensate is attractive, which energetically favors higher condensate density. The appearance of vortices, however, lowers the density of the condensate by depleting atoms in the vortex cores. Therefore, under a given rotation frequency, the number of vortices decreases as g_d is increased.

As to the excitation spectrum, a visible feature in Fig. 1 is that the frequencies of two modes denoted by the dash-dotted lines at $\omega_j/\omega_\perp = 0.7$ and 1.3 are independent of the interaction strength, which suggests that these two modes may relate to the condensate's center-of-mass motions. Indeed, by analyzing the time-dependent density of those modes, we find that the vortices remain stationary while the condensate density performs circular motion around the center of the trap. Moreover, to obtain the mode frequencies, it is convenient to consider the single-particle Hamiltonian H_0 defined in Eq. (5). After diagonalizing H_0, we obtain the Fock-Darwin levels

$$\epsilon_{n_r,m} = (|m| + 2n_r) - m\Omega, \quad (15)$$

where $n_r \geqslant 0$ and m are two integers. As we are dealing with the classical center-of-mass motion, we have ignored the zero-point energy in Eq. (15). In fact, only the lowest two frequencies, $\epsilon_{0,1} = 0.7$ and $\epsilon_{0,-1} = 1.3$, represent the dipole modes of a 2D system which possesses two degrees of freedom. Next, we consider the modes represented by the dashed lines which possess relatively high frequencies. Simple analysis reveals that these modes represent the surface excitations of the condensate. Because the DDI breaks the axial symmetry, these modes can only be roughly identified by the angular momenta of the excitations as $m \approx 2$, 3, and 4 in ascending order of the frequencies.

Finally, we examine the vortex-displacement excitations (solid lines in Fig. 1) which, in the rotating frame, represent the elliptical motions of the vortex cores around the respective equilibrium positions. Let us first consider the simplest case with a single vortex. Without DDI, the vortex core of the VDM executes a clockwise circular precession around the center of the axially symmetric trap. Such circular precession is required by the orbital angular momentum conservation and its frequency was found in several references [40–43]. In the presence of the anisotropic DDI, we find that the trajectory of the vortex core becomes an ellipse with its major axis being along the x direction, i.e., the direction of the polarized dipole moments. Moreover, as the DDI strength is increased, the ellipse becomes more eccentric.

When the ground state has two vortices, mutual interaction between vortices enriches their motions. In fact, as shown in Fig. 1, there are now two VDMs. For the low-frequency mode, two vortices move out of phase; while for the high-frequency mode, they move in phase. This observation is in agreement with that in the nondipolar condensates [44]. However, as

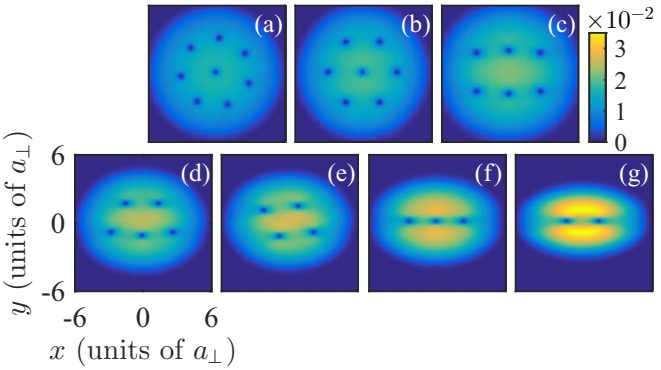

FIG. 2. Density profiles of the ground states with $\Omega = 0.5$ and for various DDI strengths. From (a) to (g), the relative dipolar interaction strengths are $g_d/g_0 = 0.005$, 0.055, 0.085, 0.12, 0.135, 0.15, and 0.175, respectively.

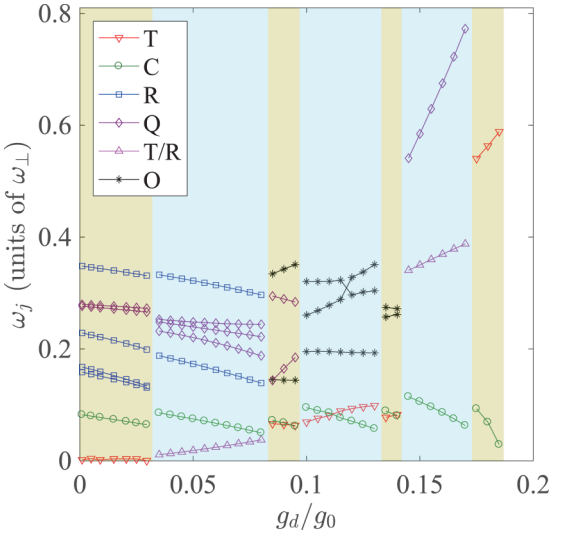

FIG. 3. Excitation frequencies of the VDMs as functions of the DDI strength. From left to right, distinct shaded regions correspond to ground states with 8, 7, 6, 5, 4, 3, and 2 vortices. T, C, Q, and R label the Tkachenko, common, quadratic, and rational modes, respectively. O denotes modes that do not fall into these four types. For the 7-, 3-, and 2-vortex states, movies of $n_p(\boldsymbol{\rho},t)$ perturbed by different modes are shown in the Supplemental Material [46].

one increases g_d, the frequency of the in-phase (out-of-phase) mode decreases (increases). Eventually, as shall be shown, the frequency of the out-of-phase mode becomes larger than that of the in-phase mode (see Fig. 3).

B. Vortex-displacement excitations

In this section, we shall focus on the VDMs in the rotating condensates. To this end, we increase the rotation frequency to $\Omega = 0.5$ such that the condensate contains more vortices. Figure 2 shows the density profiles of the ground states under various DDI strengths. As can be seen, the number of vortices N_v drops from $N_v = 8$ to 2 when g_d is increased gradually. In the weak DDI limit with $N_v = 8$ and 7, the vortices form a pattern with $N_v - 1$ vortices located on a ring plus one vortex at the center. However, with growing g_d, the pattern of the vortices may deviate significantly from the triangular lattices in the nondipolar condensates. As an example, for the three-vortex state in Fig. 2(f), instead of forming an equilateral triangle as in the nondipolar case, all three vortices evenly distribute over a line segment on the x axis with the middle vortex located at the center of the trapping potential. This result is in agreement with the previous study [25].

For a many-vortex state, the number of VDMs is equal to the number of vortices [18]. These VDMs, according to Campbell [45] and Simula [18], can be classified into four types that are briefly summarized as follows. The common mode (C) refers to the center-of-mass excitation of the vortices. In the frame corotating with the trapping potential, the whole vortex array of the common mode executes retrograde circular motion around the trap center as a rigid body. We note that the common mode is shared by all vortex configurations. The Tkachenko mode (T) is another universal collective excitation which reveals itself as a torsional oscillation of the vortex lattice around the trap center. In nondipolar condensates, the Tkachenko mode typically has the lowest excitation energy. When the condensate consists of a ring of vortices and a central single vortex (or a cluster of vortices), the quadratic modes (Q) appear for which the central vortex executes rigid-body oscillation while the vortices in the ring are able to move relative to each other. Finally, the rational modes (R) refer to motion of the vortices with the central vortex remaining stationary.

Figure 3 shows the excitation frequencies of the VDMs as functions of the dipolar interaction strength for rotation frequency $\Omega = 0.5$. Again, the spectra along the g_d axis are divided into seven regions according to the number of vortices in the condensate. For small g_d, our results are in agreement with those for nondipolar condensates. As an example, for the seven-vortex state, the excitation spectrum is very similar to that obtained in Ref. [18] for a nondipolar condensate except that the fourth lowest mode is now a rational mode as compared to the quadratic one. In addition, the Tkachenko mode has a lower excitation energy than that of the common mode. When the DDI strength is increased, vortices do not form a ring pattern, consequently, some of the VDMs cannot be described by the four types of modes introduced above. Another feature different from these results in Ref. [18] is that the common modes may have the lowest excitation energy. As the number of vortices continuously drops to three and two with increasing g_d, the situation becomes much simpler. For the three-vortex state, the lowest excitation is a common mode for which all three vortices execute the elliptic motion around the respective equilibrium position simultaneously. For the next mode with higher frequency, the vortex at the center remains stationary, while two endpoint vortices execute mutually out-of-phase motion, in analog to the out-of-phase mode in the two-vortex state. Therefore, this mode can be categorized as either Tkachenko or rational mode. For the highest frequency mode, the center vortex executes the clockwise elliptic motion, while two endpoint vortices move anticlockwise, indicating that it is a quadratic mode. Finally, for the two-vortex state, the in-phase (common) mode now has lower excitation energy than the out-of-phase (Tkachenko) mode.

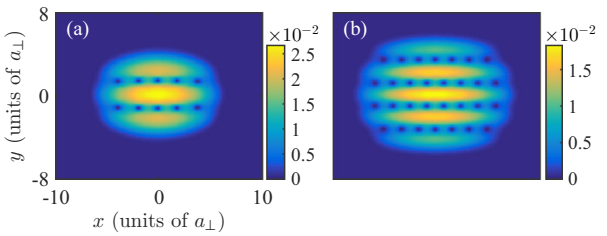

FIG. 4. Density profiles of the ground states under the DDI strength $g_d/g_0 = 0.15$ for $\Omega = 0.7$ (a) and 0.9 (b).

C. Low-lying excitations at the strong DDI limit

In the strong DDI limit, the condensate is significantly stretched along the x axis. Then, under sufficiently large rotation frequency, vortices form striped lattices such that the intervortex spacing along the x axis is smaller than that along the y axis. In Fig. 4, we present the typical density profiles for striped vortex lattices with $g_d/g_0 = 0.15$ and under two different rotation frequencies $\Omega = 0.7$ and 0.9. Correspondingly, Table I lists the frequencies of the low-excitation modes, which can be analyzed by decomposing a collective motion into the intra-row and inter-row excitations.

Let us first consider the lower rotation frequency case with $\Omega = 0.7$. This condensate contains ten vortices that are evenly divided into two rows. For a five-vortex row, the intra-row VDMs can also be described by the terms introduced in Sec. III B. Interestingly, a different type of common mode (C′) appears for which all vortices roughly execute horizontal oscillations. It should also be noted that since both rows are away from the trap center, the intra-row Tkachenko mode now represents the torsional oscillation of the row around the center of the row, instead of the trap center. For low-lying collective excitations, it is found numerically that the intra-row excitation modes are always the same for both rows. As to the inter-row excitations, there are only two types of relative motion between rows: in-phase (i) and out-of-phase (o) motions. Therefore, we may denote a VDM with an upper-case letter for the intra-row excitation accompanied by a lower-case letter (in parentheses) for the inter-row motion (see Table I). To visualize these modes, we plot, in Fig. 5, the instantaneous density profiles perturbed by different VDMs. As can be seen, the notation introduced above indeed captures the features of the VDMs in this system. In particular, since both rows in the C′(o) mode execute horizontal motion, mode 2 actually represents the inter-row shearing motion. For convenience, we also present the movies of $n_p(\boldsymbol{\rho},t)$ for all modes listed in Table I in the Supplemental Material [46].

TABLE I. Frequencies of the low-lying excitations for $\Omega = 0.7$ (left column) and 0.9 (right column). The DDI strength is $g_d/g_0 = 0.15$. The notation labeling the different excitations is explained in the main text. Movies showing the dynamical behavior of all listed modes can be found in the Supplemental Material [46].

$\Omega = 0.7$			$\Omega = 0.9$		
Mode	$\omega_q(\omega_\perp)$	Label	Mode	$\omega_q(\omega_\perp)$	Label
1	0.0415	C(i)	1	0.0088	C(iii)
2	0.0684	C′(o)	2	0.0216	C′(ioi)
3	0.2517	T(i)	3	0.0519	C′(oio)
4	0.3000	Dipole	4	0.0576	C′(ooo)
5	0.3271	T(o)	5	0.1000	Dipole
6	0.5170	Q(i)	6	0.1176	T(iii)
7	0.5489	Surface	7	0.1583	T(ioi)
7′	0.5489	Surface	8	0.1999	T(oio)
8	0.5750	Q(o)	9	0.2233	T(ooo)
9	0.5803	Surface	10	0.2442	Surface
10	0.7717	Surface	11	0.2801	Surface
11	0.7744	R(o)	11′	0.2801	Surface
12	0.7885	Surface	12	0.2931	Q(iii)
12′	0.7885	Surface	13	0.3216	Q(ioi)
13	0.8207	R(i)	14	0.3507	Q(ooo)
14	0.8838	Surface	15	0.3521	Q(oio)
15	0.9343	Surface	16	0.3959	Mixed
16	0.9617	Surface	17	0.4223	Mixed
17	0.9778	Mixed	18	0.4491	Mixed
18	0.9934	Mixed	19	0.4544	Surface
19	1.0153	Mixed	19′	0.4544	Surface
20	1.0330	Mixed	20	0.4932	Mixed

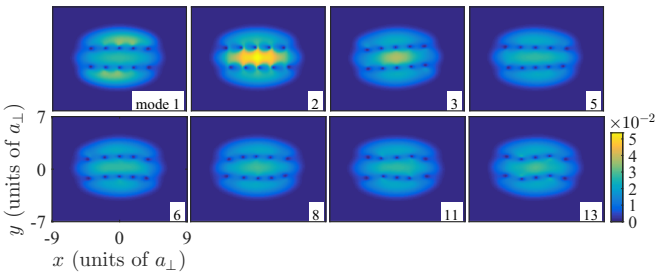

FIG. 5. Snapshots of the density profiles $n_p(\boldsymbol{\rho},t)$ [Eq. (14)] perturbed by different excitation modes. Other parameters are $g_d/g_0 = 0.15$ and $\Omega = 0.7$.

One should note that, in Table I, some of the modes do not belong to the VDM. For example, mode 4 is a dipole mode whose frequency is exactly that obtained with Eq. (15). Modes 7 and 7′ are two degenerate surface modes, for which the positions of the vortices remain stationary. To gain more insight into these modes, we plot $|u_7(\boldsymbol{\rho})|^2$ and $|v_7(\boldsymbol{\rho})|^2$ in Figs. 6(a) and 6(b), respectively. As can be seen, u_7 and v_7 only occupy two separated regions that are away from the center of the condensate where $n_0(\boldsymbol{\rho})$ is very small. Therefore, only the surface of the condensate is perturbed by the excitation, while all vortices remain unperturbed by the excitation (see Supplemental Material [46]). Additionally, the fact that $|u_7|^2$ and $|v_7|^2$ are highly anisotropic suggests that mode 7 is a superposition of many surface modes with different angular momenta. It should also be noted that in Table I, we can only identify eight VDMs although ten are expected. It turns out that some VDMs with higher excitation frequency are coupled to the surface mode. As a concrete example, we consider mode 17 whose mode functions $|u_{17}(\boldsymbol{\rho})|^2$ and $|v_{17}(\boldsymbol{\rho})|^2$ are plotted in Figs. 6(c) and 6(d), respectively. The fact that $|u_{17}| \gg |v_{17}|$ allows us to focus on u_{17} for the perturbed density n_p. To analyze these mode functions, we note that for a pure VDM, $u(\boldsymbol{\rho})$ is nonzero only in the vicinities of vortex cores, because only the positions of the vortex cores are supposed to be perturbed by $u(\boldsymbol{\rho})$. Figure 6(c) instead shows

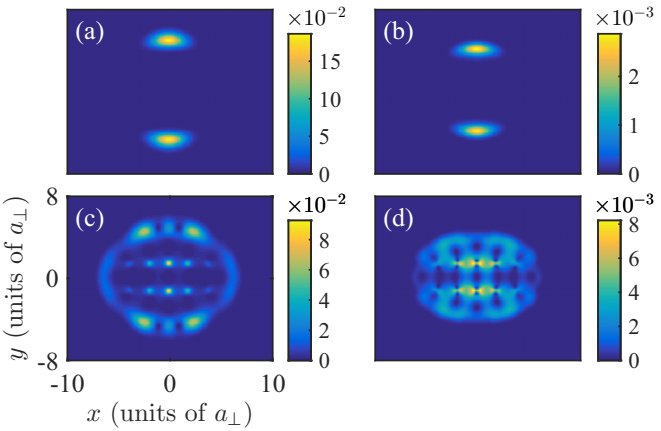

FIG. 6. Excitation mode functions $|u_j(\boldsymbol{\rho})|^2$ (left panels) and $|v_j(\boldsymbol{\rho})|^2$ (right panels) for $j = 7$ (upper panels) and 17 (lower panels). Other parameters are $g_d/g_0 = 0.15$ and $\Omega = 0.7$.

that u_{17} is nonzero not only in the vicinities of the vortex cores, but also at the surface of the condensates. Therefore, mode function u_{17} represents a superposition of VDM and surface modes.

Finally, for $\Omega = 0.9$, the ground state contains 30 vortices which are divided into four rows. It is found that the notation introduced for the VDMs in the $\Omega = 0.7$ case is still applicable except that we now need three lower-case letters (see Table I) to describe the relative motions of the neighboring rows. Of particular interest, the excitations within the lowest two sets of VDMs (C and T) are arranged according to iii, ioi, oio, and ooo in ascending order of the frequency, indicating that it costs more energy to excite the out-of-phase inter-row motions. In fact, the out-of-phase inter-row excitations unavoidably change the inter-row vortex spacing. Then, because the DDI interaction is repulsive along the y, it is natural to find that out-of-phase inter-row motions cost more energy.

IV. CONCLUSIONS

In conclusion, we have numerically studied the low-lying collective excitations of a quasi-2D rotating condensate with anisotropic dipolar interaction. We have shown how the excitation spectra of the vortex states depend on trap rotation frequency and DDI strength. In the fast-rotating and strong DDI limit, vortices form stripe lattices due to the broken rotational symmetry. As a result, the low-lying Tkachenkon waves take the form of various shearing motions between neighboring rows, which is distinct from Tkachenkon modes of conventional vortex lattices with isotropic interactions. Moreover, for excitations with higher energy, Tkachenkon modes also couple to the surface modes due to the anisotropic DDI. Since our results cover the parameter regime accessible to current experiments, we hope this study will stimulate experimental efforts aimed at observing Tkachenkon waves in dipolar condensates.

ACKNOWLEDGMENTS

This work was supported by the NSFC (Grants No. 11434011, No. 11674334, and No. 11747601) and by the Key Research Program of the Chinese Academy of Sciences (Grant No. XDPB08-1).

[1] E. B. Sonin, Vortex oscillations and hydrodynamics of rotating superfluids, Rev. Mod. Phys. **59**, 87 (1987).
[2] L. M. Pismen, *Vortices in Nonlinear Fields* (Clarendon, Oxford, 1999).
[3] For a review, see B. A. Malomed *et al.*, Spatiotemporal optical solitons, J. Opt. B **7**, R53 (2005).
[4] M. R. Matthews, B. P. Anderson, P. C. Haljan, D. S. Hall, C. E. Wieman, and E. A. Cornell, Vortices in a Bose-Einstein Condensate, Phys. Rev. Lett. **83**, 2498 (1999).
[5] K. W. Madison, F. Chevy, W. Wohlleben, and J. Dalibard, Vortex Formation in a Stirred Bose-Einstein Condensate, Phys. Rev. Lett. **84**, 806 (2000).
[6] E. Hodby, G. Hechenblaikner, S. A. Hopkins, O. M. Marago, and C. J. Foot, Vortex Nucleation in Bose-Einstein Condensates in An Oblate, Purely Magnetic Potential, Phys. Rev. Lett. **88**, 010405 (2001).
[7] J. R. Abo-Shaeer, C. Raman, J. M. Vogels, and W. Ketterle, Observation of vortex lattices in Bose-Einstein condensates, Science **292**, 476 (2001).
[8] P. C. Haljan, I. Coddington, P. Engels, and E. A. Cornell, Driving Bose-Einstein Condensate Vorticity with a Rotating Normal Cloud, Phys. Rev. Lett. **87**, 210403 (2001).
[9] For a review, see, for example, A. L. Fetter, Rotating trapped Bose-Einstein condensates, Rev. Mod. Phys. **81**, 647 (2009).
[10] V. K. Tkachenko, Stability of vortex lattices, Sov. Phys. JETP **23**, 1049 (1966).
[11] C. D. Andereck and W. I. Glaberson, Tkachenko waves, J. Low Temp. Phys. **48**, 257 (1982).
[12] I. Coddington, P. Engels, V. Schweikhard, and E. A. Cornell, Observation of Tkachenko Oscillations in Rapidly Rotating Bose-Einstein Condensates, Phys. Rev. Lett. **91**, 100402 (2003).
[13] G. Baym, Tkachenko Modes of Vortex Lattices in Rapidly Rotating Bose-Einstein Condensates, Phys. Rev. Lett. **91**, 110402 (2003).
[14] T. Mizushima, Y. Kawaguchi, K. Machida, T. Ohmi, T. Isoshima, and M. M. Salomaa, Collective Oscillations of Vortex Lattices in Rotating Bose-Einstein Condensates, Phys. Rev. Lett. **92**, 060407 (2004).
[15] S. J. Woo, L. O. Baksmaty, S. Choi, and N. P. Bigelow, Excitation Spectroscopy of Vortex Lattices in a Rotating Bose-Einstein Condensate, Phys. Rev. Lett. **92**, 170402 (2004).
[16] L. O. Baksmaty, S. J. Woo, S. Choi, and N. P. Bigelow, Tkachenko Waves in Rapidly Rotating Bose-Einstein Condensates, Phys. Rev. Lett. **92**, 160405 (2004).

[17] T. P. Simula and K. Machida, Kelvin-Tkachenko waves of few-vortex arrays in trapped Bose-Einstein condensates, Phys. Rev. A **82**, 063627 (2010).
[18] T. Simula, Collective dynamics of vortices in trapped Bose-Einstein condensates, Phys. Rev. A **87**, 023630 (2013).
[19] A. Griesmaier, J. Werner, S. Hensler, J. Stuhler, and T. Pfau, Bose-Einstein Condensation of Chromium, Phys. Rev. Lett. **94**, 160401 (2005).
[20] Q. Beaufils, R. Chicireanu, T. Zanon, B. Laburthe-Tolra, E. Maréchal, L. Vernac, J.-C. Keller, and O. Gorceix, All-optical production of chromium Bose-Einstein condensates, Phys. Rev. A **77**, 061601(R) (2008).
[21] M. Lu, N. Q. Burdick, S. H. Youn, and B. L. Lev, Strongly Dipolar Bose-Einstein Condensate of Dysprosium, Phys. Rev. Lett. **107**, 190401 (2011).
[22] K. Aikawa, A. Frisch, M. Mark, S. Baier, A. Rietzler, R. Grimm, and F. Ferlaino, Bose-Einstein Condensation of Erbium, Phys. Rev. Lett. **108**, 210401 (2012).
[23] N. R. Cooper, E. H. Rezayi, and S. H. Simon, Vortex Lattices in Rotating Atomic Bose Gases with Dipolar Interactions, Phys. Rev. Lett. **95**, 200402 (2005).
[24] J. Zhang and H. Zhai, Vortex Lattices in Planar Bose-Einstein Condensates with Dipolar Interactions, Phys. Rev. Lett. **95**, 200403 (2005).
[25] S. Yi and H. Pu, Vortex structures in dipolar condensates, Phys. Rev. A **73**, 061602 (2006).
[26] B. C. Mulkerin, R. M. W. van Bijnen, D. H. J. O'Dell, A. M. Martin, and N. G. Parker, Anisotropic and Long-Range Vortex Interactions in Two-Dimensional Dipolar Bose Gases, Phys. Rev. Lett. **111**, 170402 (2013).
[27] R. M. Wilson, S. Ronen, and J. L. Bohn, Stability and excitations of a dipolar Bose-Einstein condensate with a vortex, Phys. Rev. A **79**, 013621 (2009).
[28] D. H. J. O'Dell and C. Eberlein, Vortex in a trapped Bose-Einstein condensate with dipole-dipole interactions, Phys. Rev. A **75**, 013604 (2007).
[29] M. Abad, M. Guilleumas, R. Mayol, M. Pi, and D. M. Jezek, Vortices in Bose-Einstein condensates with dominant dipolar interactions, Phys. Rev. A **79**, 063622 (2009).
[30] R. M. W. van Bijnen, A. J. Dow, D. H. J. O'Dell, N. G. Parker, and A. M. Martin, Exact solutions and stability of rotating dipolar Bose-Einstein condensates in the Thomas-Fermi limit, Phys. Rev. A **80**, 033617 (2009).
[31] V. M. Lashkin, A. I. Yakimenko, and Yu A. Zaliznyak, Stable three-dimensional vortex solitons in Bose-Einstein condensates with nonlocal dipole-dipole interaction, Phys. Scr. **79**, 035305 (2009).
[32] C. Yuce and Z. Oztas, Off-axis vortex in a rotating dipolar Bose-Einstein condensate, J. Phys. B **43**, 135301 (2010).
[33] F. Malet, T. Kristensen, S. M. Reimann, and G. M. Kavoulakis, Rotational properties of dipolar Bose-Einstein condensates confined in anisotropic harmonic potentials, Phys. Rev. A **83**, 033628 (2011).
[34] R. Kishor Kumar and P. Muruganandam, Vortex dynamics of rotating dipolar Bose-Einstein condensates, J. Phys. B **45**, 215301 (2012).
[35] Y. Zhao, J. An, and C.-D. Gong, Vortex competition in a rotating two-component dipolar Bose-Einstein condensate, Phys. Rev. A **87**, 013605 (2013).
[36] S. Ronen, D. C. E. Bortolotti, and J. L. Bohn, Bogoliubov modes of a dipolar condensate in a cylindrical trap, Phys. Rev. A **74**, 013623 (2006).
[37] A. D. Martin and P. B. Blakie, Stability and structure of an anisotropically trapped dipolar Bose-Einstein condensate: Angular and linear rotons, Phys. Rev. A **86**, 053623 (2012).
[38] S. Giovanazzi, A. Görlitz, and T. Pfau, Tuning the Dipolar Interaction in Quantum Gases, Phys. Rev. Lett. **89**, 130401 (2002).
[39] R. B. Lehoucq, D. C. Sorensen, and C. Yang, ARPACK *Users' Guide* (SIAM, Philadelphia, 1998).
[40] B. Y. Rubinstein and L. M. Pismen, Vortex motion in the spatially inhomogenous conservative Ginzburg-Landau model, Physics D **78**, 1 (1994).
[41] A. A. Svidzinsky and A. L. Fetter, Stability of a Vortex in a Trapped Bose-Einstein Condensate, Phys. Rev. Lett. **84**, 5919 (2000).
[42] E. Lundh and P. Ao, Hydrodynamic approach to vortex lifetimes in trapped Bose condensates, Phys. Rev. A **61**, 063612 (2000).
[43] S. Middelkamp, P. G. Kevrekidis, D. J. Frantzeskakis, R. Carretero-González, and P. Schmelcher, Bifurcations, stability, and dynamics of multiple matter-wave vortex states, Phys. Rev. A **82**, 013646 (2010).
[44] T. P. Simula, A. A. Penckwitt, and R. J. Ballagh, Giant Vortex Lattice Deformations in Rapidly Rotating Bose-Einstein Condensates, Phys. Rev. Lett. **92**, 060401 (2004).
[45] L. J. Campbell, Transverse normal modes of finite vortex arrays, Phys. Rev. A **24**, 514 (1981).
[46] See Supplemental Material at http://link.aps.org/supplemental/10.1103/PhysRevA.97.043614 for the movies of low-lying excitation modes of the selected vortex states.